Analysis of Blackbody-Like Radiation from Laser-Heated Gas-Phase Tungsten Nanoparticles

Lars Landström*

The Ångström Laboratory, Department of Materials Chemistry, Uppsala University, Box 538, S-751 21 Uppsala, Sweden

Peter Heszler†

The Ångström Laboratory, Department of Solid State Physics, Uppsala University, Box 534, S-751 21 Uppsala, Sweden

Received: September 16, 2003; In Final Form: November 6, 2003

Thermal (blackbody-like) radiation that originated from laser-heated tungsten nanoparticles was measured using optical emission spectroscopy. The nanoparticles were generated via ArF excimer laser-assisted photolytic decomposition of $WF_6/H_2/Ar$ gas mixtures, and the laser heating was applied parallel to the deposition. The temperature of the nanoparticles was determined, and its dependence on time, with respect to the 15-ns laser pulse (full width at half-maximum, fwhm) and laser fluence (ϕ), has been presented. At $\phi > 90$ mJ/cm^2, the particles reached the melting point (shortly after the laser pulse). Dominant cooling mechanisms, such as evaporation (above ~3000 K) and a combination of heat transfer by the ambient gas and radiative cooling (below ~3000 K), were observed for the nanoparticles, which were ~10 nm in diameter. The degree of inelasticity for the (predominantly) argon-gas collisions and the total emissivity of the particles (in the 2500−3000 K temperature region) could also be derived. The measured cooling rate and temperature data indicate that, depending on experimental parameters, evaporation and surface reactions can have a definite effect on the growth of particles.

Introduction

Nanoparticles have attracted the attention of an increasing number of researchers within different areas of materials science during the past few years. Nanoparticles, and materials that are composed of nanoparticles, primarily exhibit different and superior properties (e.g., chemical, electronic, optical, and magnetic), compared to the bulk; these properties make them interesting and promising for various applications.[1,2]

Nanoparticles can be produced using a vast number of methods,[3] and vapor condensation techniques (chemical, physical, etc.), where the particles are formed from an oversaturated vapor, are among the most common. In this report, laser-assisted chemical vapor deposition (LCVD) has been used to generate tungsten nanoparticles from $WF_6/H_2/Ar$ gas mixtures. The particles are formed via homogeneous nucleation in the gas phase, and, because a pulsed laser is used, subsequent laser pulses will heat the aerosol particles. Thermal radiation that originates from these laser-excited particles can be recorded by means of optical emission spectroscopy (OES), and the temperature of the particles can then be determined.[4] If a gateable detector is used, information on the emitted intensity and temperature, with respect to time, can also be extracted.

The temperature of the laser-heated particles, as a function of time—with respect to the laser excitation—and laser fluence was investigated to follow and understand the different cooling mechanisms of the hot nanoparticles. Knowledge of the temperature of the laser-heated particles and the rate of cooling is of great interest, to understand and control the physical and chemical processes that govern the particle formation. For example, most surface processes (e.g., desorption, deposition, and evaporation) are strongly temperature-dependent and will, of course, affect the final mean size and even the size distribution of the generated particles. In addition, by controlling the rate of quenching, the crystallization of the particles can be controlled; e.g., high rates of cooling can produce glassy structures and/or metastable high-temperature phases. Furthermore, if the particles reach the melting point, a more effective recrystallization is expected (if lower rates of quenching are used).

Because one of the cooling mechanisms is heat transfer by inelastic collisions with the ambient gas, the degree of inelasticity (accommodation factor) of the collisions could also be determined. In addition, the intensity decay of the thermal radiation over time gave information about quenching effects, which are also related to ambient gas collisions.

Finally, it is also noted that thermal radiation and thermionic electron emission from small tungsten clusters (cluster sizes up to 200 atoms) have already been observed experimentally.[5,6]

Experimental Section

The experimental setup consisted of a stainless-steel vacuum chamber with quartz windows at the front (laser-beam in) and on top of the reactor. The flowthrough reactor had a cross section of ~12 cm^2, and the laser-induced light emission was observed perpendicular to the laser beam through the top window of the chamber and was coupled to a quartz optical fiber attached to the optical detection system. Furthermore, two apertures (each

* Author to whom correspondence should be addressed. Telephone: +46 (0)18 471 3769. Fax: +46 (0)18 513 548. E-mail: address: Lars.Landstrom@mkem.uu.se.

† Also with the Research Group on Laser Physics of the Hungarian Academy of Sciences, Szeged, Box 406, H-6721, Hungary.

10.1021/jp0367629 CCC: $27.50
Published on Web 04/21/2004

with $d = 1$ cm and separated by ~2 cm) were mounted inside the reactor and in front of the top window, to prevent the deposition of tungsten.

A Czerny−Turner-type grating spectrograph, a charge-coupled device (CCD) detector, and an optical multichannel analyzer (model OMA III, from EG&G) were used as the optical detection system. The CCD detector was gateable, with a minimum gate pulse length of 100 ns; therefore, time-resolved spectroscopy on the microsecond time scale could be performed. The overall exposure time was set to either 1 or 2 s (an exposure time of 2 s was used to obtain better statistics for weaker emissions). A 150 lines/mm grating allowed a spectral resolution of 1.8 nm and a wavelength accuracy of ±0.2 nm.

The relative transfer function of the detection system was determined using a tungsten-strip calibration lamp, and that of the emissivity variation over the visible region was <0.5%. Measured spectra were corrected by the relative transfer function and, to determine the temperature of the nanoparticles, were fitted using the relation

$$N_p(\lambda) \propto \frac{1}{\lambda^{5.43}}\left(\frac{1}{\exp[hc/(\lambda k_B T)] - 1}\right) \quad (1)$$

where λ is the wavelength of the emitted radiation, $N_p(\lambda)$ denotes the photon number in the $(\lambda, \lambda + \Delta\lambda)$ spectral region (note that the CCD detector counts the photon number), h is Planck's constant, c is the speed of light, k_B is the Boltzmann constant, and T is the absolute temperature. Equation 1 involves the emissivity of tungsten nanoparticles, which was proportional to $\lambda^{-1.43}$ in the observed spectral region (400−700 nm).[4]

Integrated intensity data were obtained by summation of the emitted radiation in the observed wavelength window. It is also noted that the temperature differs by, at the most, ~20% in the performed experiments, so λ_{max} (the wavelength at maximum intensity) in the corresponding Planck curve changes by a maximum of 20%. Therefore, the change of intensity in the observed wavelength window, because of a red or blue shift, was neglected during experiments.

$WF_6/H_2/Ar$ gas compositions, in a molar ratio of 1/3/90, were used at total pressures in the range of 5−80 mbar, with a constant linear velocity of 3.3 cm/s; i.e., the gas flows were scaled at the different pressures to obtain the same linear velocity.

The laser parameters were as follows: wavelength, 193 nm (Lambda Physik ArF excimer laser); nominal pulse duration, 15 ns (full width at half maximum, fwhm); and repetition rate, 50 Hz. The laser fluence (ϕ) was set to 120 mJ/cm^2 at a total pressure (p_{tot}) of 20 mbar for the time-resolved spectroscopy, and ϕ was varied within a range of 40−140 mJ/cm^2 at $p_{tot} =$ 20 mbar to measure its effect on the light emission and temperature of the particles. (The laser beam cross section, at the place of optical observation, was 2 cm × 0.5 cm.)

During the experiments, particles were deposited on carbon-covered copper grids for analysis via transmission electron microscopy (TEM).

Results

Tungsten nanoparticles were generated by UV LCVD from a $WF_6/H_2/Ar$ gas mixture. A bright-field (BF) TEM image of the deposited particles is shown in Figure 1, with an electron diffraction pattern as an inset. Calculated d-values from the ring pattern correspond well to β-tungsten, which is a metastable phase that is assumed to be stabilized by impurities (e.g., fluorine[7] and oxygen[8]). Traces of fluorine and oxygen contamination were detected using energy-dispersive X-ray spectroscopy (EDS), which supports the idea of impurity stabilization.

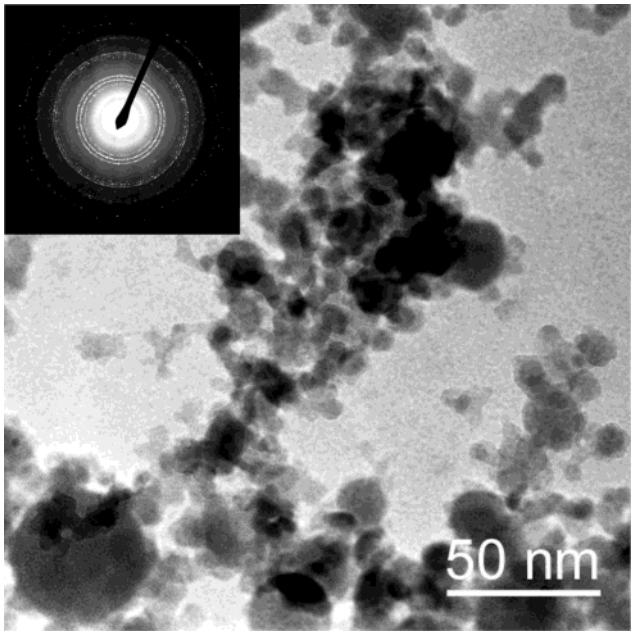

Figure 1. Bright-field transmission electron microscopy (BF TEM) image of tungsten particles deposited by laser-assisted chemical vapor deposition (LCVD) from a $WF_6/H_2/Ar$ gas mixture, with an electron diffraction pattern as the inset. Total pressure was $p_{tot} = 20$ mbar and laser fluence was $\phi = 140$ mJ/cm^2.

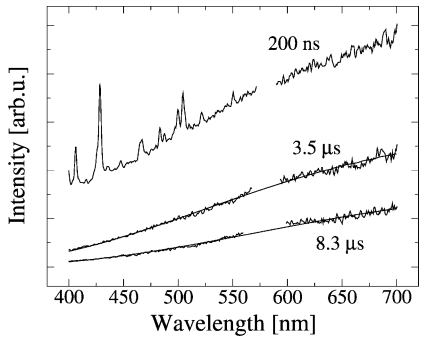

Figure 2. Time-resolved spectra originating from laser-heated tungsten nanoparticles for different delay times, with respect to the laser pulse. Total pressure was 20 mbar, laser fluence was 120 mJ/cm^2, and the gate pulse was 100 ns. Solid smooth lines (in 3.5- and 8.3-μs delay curves) are the best Planck curve fits, according to eq 1. Strong peaks at 579 nm (third-order laser line), due to the dark current in the CCD detector from the strongly scattered laser light, were cut and not considered for the fitting. Fitted temperature data: delay at 3.5 μs was 3075 K and at 8.3 μs was 2825 K. At a delay of 200 ns, superimposed elemental tungsten lines on the thermal radiation can be observed.

Typical corrected OES spectra that originated from the laser-excited nanoparticles are shown in Figure 2 for different delay times, with respect to the laser pulse. The fitted solid lines represent Planck curves according to eq 1, showing that the radiation that originates from the laser-excited particles is thermal. However, spectral lines were superimposed on the thermal radiation at early delays (<0.5 μs, Figure 2; 200 ns delay), and these lines were identified as atomic tungsten emission lines.

The temperature of the particles and intensity of the thermal radiation are shown in Figure 3a and 3b, respectively, as a function of delay time. Intensity data for longer delays (where an exposure time of 2 s was used) were normalized to an overall exposure time of 1 s. The dashed line in Figure 3a is the

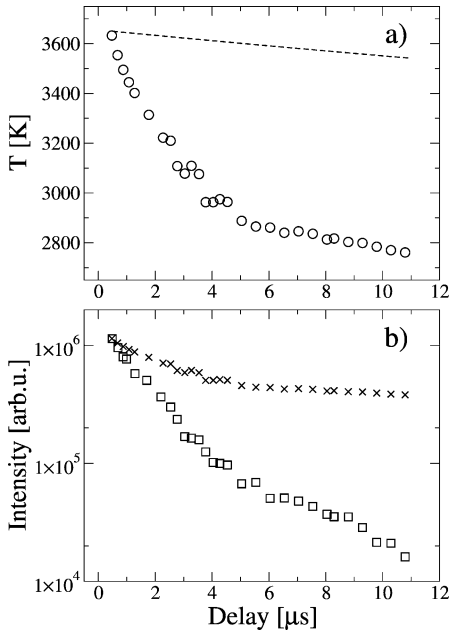

Figure 3. (a) Temperature of the nanoparticles and (b) intensity of the thermal radiation, each as a function of delay time. Dashed line in Figure 3a represents the temperature decay, assuming only radiative cooling, and data points marked by a cross (×) in Figure 3b were calculated according to the Stefan−Boltzmann law (relative to the earliest delay), using the measured temperature data displayed in Figure 3a. Gate pulse was 100 ns, total pressure was 20 mbar, and laser fluence was 120 mJ/cm^2. Note that the first data point is located at a delay of 0.5 μs. Particle mean diameter was 10 nm (see Figure 5).

calculated decay of temperature, assuming a tungsten particle 10 nm in diameter that cools purely by thermal radiation (see eq 6, presented later in this work).

Figure 3a shows that the initial derived temperature (at a delay of 0.5 μs, when no elemental lines interfered with the fitting procedure) was ∼3650 K, which is similar to the melting point of tungsten (∼3695 K). This value at 0.5 μs, combined with the rate of decrease of temperature at the earliest delays (∼300 K/μs), shows that the particles are, at least partially, melted (at a laser fluence of ϕ = 120 mJ/cm^2 in this case) during—and a short time after—the laser pulse. Also note that, because the gate pulse used was 100 ns, an average temperature during that time is recorded. Furthermore, the observed laser-excited volume was ∼0.5 cm^3, and possible temperature variations within this volume can be considered to be negligible. Moreover, similar conditions can be assumed for each laser pulse, because a steady-state concentration of particles is maintained, and the nanoparticles also have sufficient time to cool to the surrounding ambient temperature between laser pulses (20 ms between pulses at 50 Hz), as can be inferred from Figure 3a. The plotted decrease in temperature shows an initially fast (slightly declining) rate of decrease (for delays of $<$4 μs) and a slower component at longer delays ($>$4 μs).

The data points marked with a cross (×) in Figure 3b were calculated according to the Stefan−Boltzmann radiation law, using the measured temperature data that was depicted in Figure 3a. The calculations were normalized, relative to the maximum measured intensity at the earliest delay. The decrease in intensity of the thermal radiation also has two components (see Figure 3b). For the first 4 μs, the rate constant (i.e., reciprocal lifetime) is ∼1 × 10^6 s^{-1}, whereas the rate constant for the second part (the 4−11 μs range) is ∼2 × 10^5 s^{-1}.

The rate of temperature decrease (dT/dt) for the slow component (below ∼3000 K), which was approximated to be

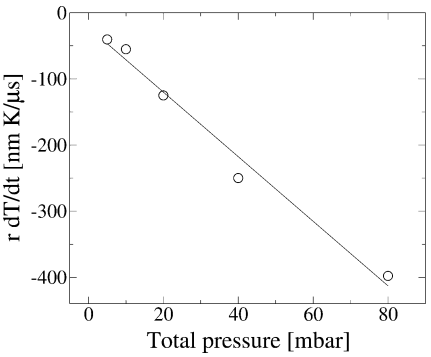

Figure 4. Product of particle mean radius (r) and rate of decrease of temperature (dT/dt) for the slow component (see, e.g., Figure 3a) for different total pressures of the $WF_6/H_2/Ar$ gas mixtures. Solid line is the best linear fit, with a slope of −5 K nm mbar^{-1} μs^{-1}. Laser fluence was 120 mJ/cm^2.

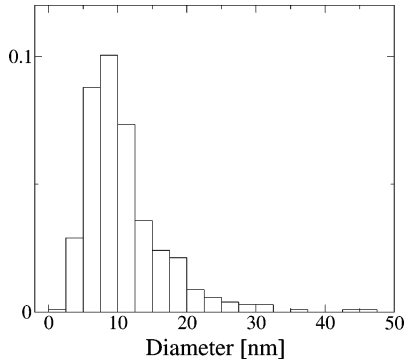

Figure 5. Normalized size distribution at a total pressure of 20 mbar and a laser fluence of 120 mJ/cm^2. Fitted geometric mean diameter was $d_g \approx$ 10 nm.

TABLE 1: Dependence of Geometric Mean Diameter on Total Pressure at Constant Laser Fluence and on Laser Fluence at Constant Total Pressure

parameter	value				
At ϕ = 120 mJ/cm^2					
total pressure, p_{tot} (mbar)	5	10	20	40	80
geometric mean diameter, d_g (nm)	6.5	8	10	13	16
At p_{tot} = 20 mbar					
laser fluence, ϕ (mJ/cm^2)	45	65	90	120	140
geometric mean diameter, d_g (nm)	8	9	9	10	9

linear, multiplied by the mean particle radius (r), versus different total pressures is depicted in Figure 4. The derivative of the fitted line in Figure 4 can be related to the cooling (heat transfer) of the particles by inelastic collisions with the ambient gas (see eq 5 in the Discussion section of this work). Geometric mean diameters of the particles (d_g) at different total pressures were obtained by measuring particle diameters (sampling size of $>$400) from BF TEM micrographs, and the results can be observed in Table 1. At a total pressure of p_{tot} = 20 mbar (corresponding to a WF_6 partial pressure of ∼20 Pa) and a laser fluence of ϕ = 120 mJ/cm^2, which are the conditions at which the time-resolved measurements were performed, a log-normal size distribution was observed (Figure 5) with a geometric mean diameter of $d_g \approx$ 10 nm.

The temperature of the particles starts to saturate above ∼90 mJ/cm^2 as the value of ϕ is increased (see Figure 6). The saturation temperature is ∼3650 K, i.e., similar to the melting temperature of tungsten. As mentioned previously, atomic tungsten lines were superimposed on the OES curves at early delays ($<$0.5 μs). A delay of 0.5 μs was used to avoid this superposition, and to obtain a better fit for the Planck curves.

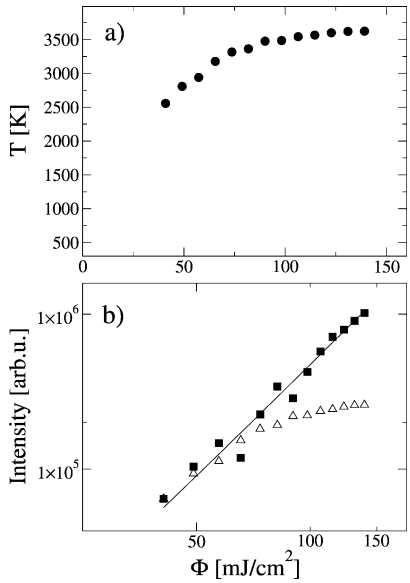

Figure 6. (a) Temperature (T) of the nanoparticles (gate pulse of 100 ns, delay of 0.5 μs, and total pressure of 20 mbar) and (b) intensity of emitted thermal radiation (I), each as a function of laser fluence ϕ. Fitted solid line gives $I \propto \phi^{2.3}$. Data marked by an open triangle (△) in Figure 6b were calculated according to the Stefan−Boltzmann law (normalized to the lowest measured intensity), using the measured temperature data displayed in Figure 6a. (Note the log−log scale on the intensity curve in Figure 6b.)

An increase of intensity of the thermal emission with ϕ can be observed in Figure 6b, and the intensity was proportional to $\phi^{2.3}$. In addition, d_g values at five different fluences were obtained by measuring particles (sampling size of >400) from BF TEM micrographs (see Table 1).

Temperatures below ~2500 K could not be monitored, because of the poor statistics of the measured spectra.

Discussion

To interpret the measured data, consideration must be given to the energy-release mechanisms of nanoparticles. As it is known, free hot particles or clusters of atoms cool via three different mechanisms: (i) evaporation of atoms/molecules (unimolecular decay), (ii) thermionic electron emission, and (iii) thermal (blackbody-like) radiation. In addition, when the particles are surrounded by a gas, inelastic collisions between the particles and the ambient gas species also result in energy transfer from the particles.

First, the rates of thermionic electron emission and evaporation were calculated for a tungsten particle 10 nm in diameter, because that was the geometric mean size that corresponded to the time-resolved spectroscopic measurements. Rates of decay of these cooling mechanisms versus particle temperature are depicted in Figure 7, using the modified Richardson−Dushman formula for thermionic electron emission[9] and Klots's evaporation model.[10] Both methods were developed for nanoparticles. In regard to the activation energy for thermionic electron emission, the nth ionization potential (I_n) of a particle was used, and this parameter can be expressed as[11]

$$I_n = W_f + \frac{1}{2}\left(\frac{n^2e^2}{4\pi\epsilon_0 r}\right) \tag{2}$$

where W_f is the work function for bulk tungsten (4.57 eV), e the elementary electron charge, ϵ_0 the vacuum dielectric constant, and r the radius of the particle (5 nm, in this case). At

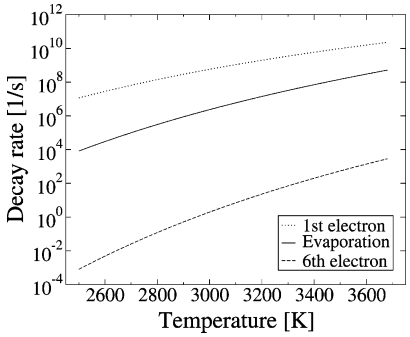

Figure 7. Calculated decay rates for thermionic electron emission and unimolecular (evaporation) decay, as a function of temperature, for a 10-nm-diameter tungsten nanoparticle.

an elevated temperature T (but below the melting temperature), the activation energy (E_a) for evaporation can be expressed as

$$E_a(T) = \frac{H_f}{N_A} - \frac{\gamma 4\pi r^2}{N_s} - \int_0^T c_a \, dT \tag{3}$$

where c_a is the atomic heat capacity, H_f the molar heat of formation, γ the surface energy for tungsten, N_A the Avogadro number, and N_s the number of surface atoms. Data were taken from literature references.[12−14] As shown in Figure 7, the rate of decay of thermionic electron emission for the first electron is ~2 orders of magnitude higher than the evaporation rate. However, the ionization potential rapidly increases with the charge state of the particles (eq 2); e.g., the decay rate for the sixth electron emission is ~6 orders of magnitude lower than that for the first electron. In addition, the emission of six electrons reduces the temperature of a 10-nm-diameter particle (at 3650 K) by only ~2 K. Thus, thermionic electron emission cannot account for the observed rate of temperature decrease (see Figure 3).

The remaining two cooling mechanisms left to discuss are heat transfer by collisions and radiative decay. The inelastic collisions between ambient atoms/molecules and the hot particles induce heat transfer as well as possible quenching of the photon emission. The energy release that is due to inelastic collisions with the ambient gas can be written as

$$c_v \frac{dT}{dt} = -\eta\xi A_S (T - T_0) \tag{4}$$

where c_v represents the heat capacity and A_S is the surface area of the particle, respectively. T_0 denotes the ambient temperature (room temperature (RT) is 295 K) and the product $\eta \times \xi$ is the heat-exchange coefficient, where ξ is the accommodation factor (a value of $\xi \leq 1$ characterizes the degree of inelasticity of the collisions). In the measured pressure range (5−80 mbar), the mean free path of argon is ~1−14 μm, i.e., much longer than the radius of the particles (see Table 1), so η can be approximated by $\eta = cJ$,[15] where c is the specific heat of the colliding species and J is the flux of atoms/molecules that are impinging on the surface of the particle. Equation 4 can then be rewritten as

$$c_v \frac{dT}{dt} = -\xi A_S (l+1)\frac{p}{T_0}\left(\frac{k_B T_0}{8\pi m_a}\right)^{1/2}(T - T_0) \tag{5}$$

where the parameter l denotes the degrees of freedom, p is the pressure, and m_a is the mass of the colliding atom/molecule. By approximating $T = 2800$ K, and using $c_v(T) \propto r^3$ and $A_S \propto r^2$, a linear curve is obtained when plotting the quantity $r \times$

dT/dt versus pressure (see Figure 4). (Geometric mean radii were used for r, to obtain better weighted values, even though the distributions at >20 mbar deviate from a log-normal distribution. This deviation is caused by increasing number of intercollisions between particles, with coalescence as a result.) The slope of the curve in Figure 4 (-5 K nm mbar^{-1} μs^{-1}) can then be used to estimate the value of ξ from eq 5. For the laser-heated tungsten nanoparticles, in the temperature range of 2600−3000 K, the accommodation factor for argon was observed to be $\xi = 0.04$ (H_2 was neglected, because of the low partial pressure).

Cooling by radiative energy loss is given by the Stefan−Boltzmann radiation law:

$$c_v \frac{dT}{dt} = -A_S \epsilon \sigma_{SB} (T - T_0)^4 \qquad (6)$$

where ϵ is the total emissivity of the particle and σ_{SB} is the Stefan−Boltzmann constant.

The total emissivity value ϵ for a 10-nm-diameter particle at a total pressure of 20 mbar could be estimated as follows. All of the cooling rates in Figure 4 were measured below ~3000 K, where evaporation rates—and cooling by thermionic electron emission—are negligible (see Figure 7). Therefore, the cooling that occurs below ~3000 K can be attributed to a combination of radiative and inelastic heat transfer, where the latter can be calculated based on the slope of curve in Figure 4. The measured dT/dt value at a total pressure of 20 mbar is ~25 K/μs at a delay of 5−11 μs. The inelastic contribution is ~20 K/μs (from the slope in Figure 4), and the remaining 5 K/μs corresponds to the radiative decay. Using eq 6, a total emissivity of $\epsilon = 0.01$ could be derived for a 10-nm-diameter tungsten particle at ~2800 K. This value was used for calculation of pure radiative decay in Figure 3a. It is also noted that calculated spectral emissivity values (in the visible-wavelength region) for a 10-nm-diameter tungsten particle, using Mie theory approximations,[16] gives an average value of ~0.03 for the visible spectral range at RT.

In regard to the cooling mechanisms, the rate of temperature decrease (dT/dt) is ~5 K/μs for radiative decay and ~20 K/μs for the heat transfer by inelastic collisions at temperatures below 3000 K. However, the measured cooling rate (see Figure 3a) is ~300 K/μs at temperatures above 3000 K (i.e., for the first 4 μs), and this value cannot be explained either by radiative cooling (dashed line in Figure 3a) or by heat transfer by the ambient gas, because the rate of the latter may increase only by ~20%, because of the increase in temperature (from 3000 K to 3600 K).

The value of dT/dt is ~300 K/μs for the first microseconds, which corresponds to an evaporation of $\sim 1 \times 10^9$ atoms per second for a 10-nm-diameter particle. The calculated rate for evaporation close to the melting point (i.e., no melting is included, which would increase the rate of evaporation) is $\sim 5 \times 10^8$ s^{-1} (see Figure 7), and, considering that the heat of fusion is not incorporated in the calculations, combined with the uncertainties of the estimations (e.g., the activation energy for evaporation can be affected by the observed fluorine and oxygen contaminants), the agreement between measured and calculated values can be considered to be very good.

It is thus concluded that (i) the evaporation of atoms is the dominant cooling mechanism at elevated temperatures (>3000 K), and (ii) a combination of radiative cooling and heat transfer by inelastic collisions is dominant at temperatures below ~3000 K.

Also note that the decay rate of intensity of the thermal radiation is higher—both for longer ($\sim 2 \times 10^5$ s^{-1}) and shorter ($\sim 1 \times 10^6$ s^{-1}) delays—by ~1 order of magnitude than the rate of decay that can be calculated from the measured temperatures depicted in Figure 3a, in accordance with the Stefan−Boltzmann law (data points marked by a cross (×) in Figure 3b). At longer delay times (5−11 μs), this difference can be explained by considering the Ar/H_2 collisions with the tungsten nanoparticles, which quench the photon emission from the hot particles with a certain probability. As mentioned previously, the inelastic collisions with ambient gas species remove energy from the particles, which also results in cooling. (A 10-nm-diameter particle collides with $\sim 1.5 \times 10^4$ Ar atoms per microsecond at an argon partial pressure of 20 mbar.)

The higher rate of decay ($\sim 1 \times 10^6$ s^{-1}) at shorter delays—and, thus, elevated temperatures (> 3000 K)—can be explained by the fact that evaporation events also quench the thermal light emission. However, the measured rate of decay of the intensity ($\sim 1 \times 10^6$ s^{-1}) is less than the observed rate of evaporation ($\sim 1 \times 10^9$ s^{-1}). This can be explained by the fact that not every evaporation of an atom quenches the light emission, because the lifetime of the electronically excited state of a particle is short (less than a nanosecond). In addition, an evaporation event occurs approximately once every nanosecond.

The saturation of temperature as the laser fluence ϕ is increased (see Figure 6a) indicates melting of the particles, and the deviation from linearity above fluences of $\phi \approx 90$ mJ/cm^2 confirms that significant cooling—due to strong evaporation—occurs at elevated temperatures (>3000 K).

The degree of melting—and even the evaporation rate—can also be estimated from Figure 6a. The linear rate of temperature increase at low fluences is ~50 K mJ^{-1} cm^2. From this information, one can estimate that the corrected temperature should be ~6050 K at $\phi \approx 120$ mJ/cm^2 (where the time-resolved spectroscopy was performed), assuming that no melting or evaporation occurs. However, the determined temperature, at a delay of 0.5 μs, is ~3650 K; that is, the temperature difference of 6050 K −3650 K, multiplied by the heat capacity of a 10-nm-diameter tungsten particle gives the amount of energy that is responsible for evaporation and melting. Calculations indicate that, for $\Delta t = 0$ (directly after the laser pulse, i.e., no evaporation is assumed), the entire particle is melted; moreover, ~3000 atoms must be evaporated to account for the energy balance at a delay of 500 ns. This value corresponds to a rate of evaporation of 6×10^9 s^{-1} and is in relatively good agreement with the number that was derived from the time-resolved measurements ($\sim 2 \times 10^9$ s^{-1}, as extrapolated to a delay of 500 ns). It can also be estimated that, because the mean particle size is a weak function of ϕ in the investigated region (see Table 1), the particles are melted at $\phi \approx 90$ mJ/cm^2.

The strong evaporation is also confirmed by the fact that elemental tungsten lines were observed at early delays (<0.5 μs), with respect to the laser pulse. This can be explained by evaporation of electronically excited W atoms by the hot particles, and de-excitation of these atoms results in the observed atomic tungsten lines (see Figure 2, 200-ns delay).

The intensity dependence on laser fluence is proportional to $\phi^{2.3}$, and a deviation can be observed from the calculated intensity, using the Stefan−Boltzmann radiation law (see Figure 6b). This discrepancy between measured and calculated values can be explained, given that the particles are similar in mean size (see Table 1), by the simple fact that more particles are produced as ϕ increases.

Conclusions

A study of thermal (blackbody-like) radiation from tungsten nanoparticles, produced by the laser-assisted photolytic decom-

position of WF_6/H_2/Ar gas mixtures, was performed. The spectra of the emitted light were detected by means of optical emission spectroscopy (OES) in the 400−700 nm wavelength range and time-resolved measurements were performed on the microsecond time scale by a gate pulse of 100 ns.

Particles produced, and excited, at a laser fluence of $\phi = 120$ mJ/cm^2 had a geometric mean diameter of $d_g \approx 10$ nm and were melted during and shortly after the laser pulse. A cooling rate of ∼300 K/μs was observed for the first several microseconds, and this observation could be attributed to the evaporation of W atoms. This time interval corresponds to a temperature range of 3650−3000 K. The strong evaporation of W atoms at elevated temperatures suggests that the size distribution can be controlled and possibly even narrowed. For example, if a fluence of $\phi = 140$ mJ/cm^2 is applied in the experimental setup that has been used (a residence time of ∼3 s and a repetition rate of 50 Hz), ∼40% of the total volume is evaporated from the laser-heated particles. Higher fluences and/or repetition rates will enhance this effect, thus decreasing the amount of bigger particulates, in accordance with evaporating the smaller features, resulting in a narrower size distribution.

Below a particle temperature of 3000 K (after a delay of ∼4 μs), heat transfer by ambient gas and thermal radiation were observed to govern the cooling process. The thermal radiation yielded a ∼5 K/μs rate of temperature decay for particles with a diameter of 10 nm in the 3000−2500 K temperature range, with an estimated overall emissivity of $\epsilon \approx 0.01$. The net effect of the ambient gas pressure on the rate of temperature decrease was ∼1 K mbar^{-1} μs^{-1} (particle diameter of 10 nm, temperature range of 3000−2500 K), with an estimated accommodation factor (degree of inelasticity) of $\xi = 0.04$ for argon.

At lower temperatures (where evaporation and desorption of surface-active species is insignificant), thermal chemical vapor deposition (TCVD) processes can contribute to the growth of the particles. The effect of this growth will be strongly dependent on the rate of cooling (dT/dt) below ∼1000 K. Using the H_2: Ar molar ratio and total pressure, the relative heat conductivity of the ambient gas mixture can be varied between 1 and ∼1000 (and, consequently, dT/dt also can be varied). This large range introduces the possibility of controlling the TCVD processes on the surface of the particles.

Thermionic electron emission was discarded as a significant cooling mechanism, becuase of the rapid increase of activation energy as the charge state of the particle increases. In addition, the emission of six electrons decreases the temperature of a 10-nm-diameter particle at 3650 K by only 2 K.

As the laser fluence ϕ was increased, the temperature of the particles saturated close to the melting point of tungsten (∼3695 K), and the deviation from a linear increase up to the saturation temperature, also confirmed the strong evaporation of W atoms at elevated temperatures.

Electron diffraction was used to identify the structure of the crystalline particles as β-tungsten, which is an impurity-stabilized metastable phase of tungsten.

Acknowledgment. Financial support from the "Swedish Research Council for Engineering Sciences" and "Göran Gustafssons Stiftelse" are gratefully acknowledged. The authors also wish to acknowledge Dr. J. Lu for operating the TEM.

References and Notes

(1) Nalwa, H. S. *Handbook of Nanostructured Materials and Nanotechnology*; Academic Press: San Diego, CA, 2000.
(2) Gleiter, H. *Acta Mater.* **2000**, *48*, 1.
(3) Hayashi, C., Uyeda, R., Tasaki, A., Eds. *Ultra-Fine Particles: Exploratory Science and Technology*; Noyes Publications: Westwood, NJ, 1997.
(4) Heszler, P.; Landström, L.; Lindstam, M.; Carlsson, J.-O. *J. Appl. Phys.* **2001**, *89*, 3967.
(5) Frenzel, U.; Hammer, U.; Westje, H.; Kreisle, D. *Z. Phys. D* **1997**, *40*, 108.
(6) Ganteför, G.; Eberhardt, W.; Weidele, H.; Kreisle, D.; Recknagel, E. *Phys. Rev. Lett.* **1996**, *77*, 4524.
(7) Tang, C. C.; Hess, D. W. *Appl. Phys. Lett.* **1984**, *45*, 633.
(8) Hägg, G.; Schönberg, N. *Acta Crystallogr.* **1954**, *7*, 351.
(9) Klots, C. E. *Chem. Phys. Lett.* **1991**, *186*, 73.
(10) Klots, C. E. *Z. Phys. D* **1991**, *20*, 105.
(11) Perdew, J. P. *Phys. Rev. B* **1988**, *37*, 6175.
(12) Chase, M. W., Jr. *NIST−JANAF Thermochemical Tables*; American Institute of Physics: Woodbury, NY, 2000.
(13) Lide, D. R., Ed. *CRC Handbook of Chemistry and Physics*, 80th ed.; CRC Press: Boca Raton, FL, 1999.
(14) Burke, J. J., Reed, N. L., Weiss, V., Eds. *Surfaces and Interfaces I*; Syracuse University Press: Syracuse, NY, 1967.
(15) Bäuerle, D. *Laser Processing and Chemistry*, 3rd ed.; Springer−Verlag: Berlin, 2000.
(16) Bohren, C. F.; Huffman, D. R. *Absorption and Scattering of Light by Small Particles*; Wiley: New York, 1983.